14th International Symposium on Turbulence and Shear Flow Phenomena (TSFP14)
Heidelberg, Germany, July 28–31, 2026

AERODYNAMIC CHALLENGES IN THE FLUID-STRUCTURE INTERACTION SIMULATION OF PARACHUTE DEPLOYMENT

Carlos Pantano
Department of Aerospace and Mechanical Engineering
University of Southern California
Los Angeles, CA 90089
pantanor@usc.edu

ABSTRACT

The fluid-structure interaction (FSI) simulation of highly deformable systems, such as parachutes, presents a confluence of challenges spanning numerical methods, physical modeling, and computational efficiency. In this paper, we examine the key aerodynamic modeling barriers to robust and predictive FSI simulation, with particular emphasis on three interrelated components. First, algorithmic and methodological challenges arise from the strong, nonlinear coupling between fluid flow and large structural deformations, often compounded by topological changes, mesh distortion, and stability constraints in both partitioned and monolithic solution strategies. Ensuring numerical stability, accuracy, and scalability under these conditions remains a central difficulty. Second, the high-Reynolds-number flows typical of parachute operation often require turbulence models to balance physical fidelity with computational tractability. The selection and integration of appropriate models (such as scale-resolving methods like large-eddy simulation) must account for their interactions with moving, highly flexible boundaries and their impact on coupling stability and solution cost; this is the focus of this paper. Third, these elements must be integrated into an efficient, scalable simulation framework that robustly resolves multiphysics interactions within practical time constraints. This requires advances in parallel algorithms, adaptive meshing, load balancing, and data management to support large-scale, high-fidelity simulations. The interplay between algorithmic design, turbulence modeling, and computational performance ultimately governs the feasibility of predictive FSI simulations for complex, real-world, descelerator systems. This paper highlights these challenges and outlines directions for developing robust, efficient, and accurate simulation methodologies for parachute deployment modeling.

1 Introduction

Parachutes have evolved from early conceptual devices intended to mitigate falls into highly engineered aerodynamic decelerators used across a wide range of civil, military, and aerospace applications. Historical accounts trace the concept to early experiments attributed to Armen Firman in the 9th century and the Renaissance sketches of Leonardo da Vinci, with the first successful demonstrations occurring in the late 18th century by L.S. Lenormand (who coined the name parachute in 1785) and A. Garnerin. Since their adoption in World War I as life-saving devices for aviators, parachutes have undergone continuous refinement, transitioning from simple fabric canopies to sophisticated systems designed for controlled deployment, stability, and performance. Modern parachutes serve diverse purposes, including personnel descent, cargo delivery, vehicle deceleration, and spacecraft recovery, all fundamentally relying on the generation of aerodynamic drag to reduce velocity.

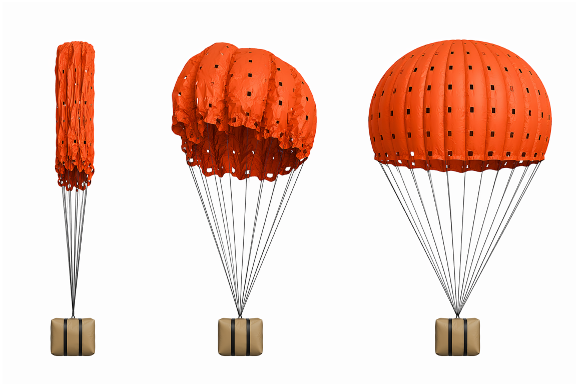

Figure 1. Sketch of prototypical parachute inflation during vertical descent. Time increases from left to right.

From a functional perspective, parachute systems can be broadly categorized into two classes: deceleration and gliding devices. The former – encompassing traditional round, ribbon, and ring-slot parachutes – operate primarily as drag-producing bodies with limited or no lift, and are widely used in recovery and descent applications where stability and predictable vertical deceleration are paramount. In contrast, modern ram-air parafoils act as lifting surfaces, enabling significant maneuverability and horizontal translation akin to gliding flight; while important, such systems fall outside the primary scope of this work. The engineering of deceleration parachutes, particularly those used in high-performance or mission-critical applications, is comprehensively documented in Knacke (1991), which provides detailed methodologies for system selection, aerodynamic performance prediction, and structural design of recovery systems. An earlier focused treatment of the aerodynamic principles governing parachutes in the subsonic regime can be found in Cockrell (1987). Together, these works frame the modern understanding of parachute aerodynamics and design, forming the basis for contemporary investigations into fluid-structure interaction in highly deformable decelerator systems.

Deployment is the critical stage in the lifecycle of a parachute: the inflation phase, initiated when the canopy is extracted from its deployment bag, often by a pilot or drogue parachute. During this process, see figure 1, the canopy undergoes a rapid geometric transformation, transitioning from a compact, folded configuration to a fully deployed aerodynamic surface through a sequence of unsteady FSI. The associated flow field is highly dynamic, characterized by large-scale separation, vortex formation, and rapidly evolving pressure distributions that strongly couple with the structural response of the fabric (Peterson *et al.*, 1996). It is within this short but violent transient that the largest dynamic loads are generated. These loads arise from rapid deceleration, canopy pressurization, and inertial effects, and are transmitted through the suspension lines into the canopy fabric.

An important mechanism for managing the severe transient loads associated with parachute deployment is reefing. Reefing is a controlled-inflation strategy in which the canopy is temporarily constrained during the early stages of deployment, typically via reefing lines or devices that limit the effective skirt diameter. As the parachute is extracted, the canopy is prevented from fully expanding, instead inflating to a reduced projected area. This staged opening allows the surrounding flow to gradually pressurize the structure while maintaining a lower initial drag force and, consequently, reduced deceleration loads. After a prescribed delay, the reefing constraint is released, either mechanically or pyrotechnically, permitting the canopy to expand to its full geometric configuration. In many applications, this process occurs in multiple stages, with successive reefing levels designed to further smooth the inflation dynamics. Reefing is critical because it directly addresses the problem of opening shock, which can otherwise generate extreme transient forces that can exceed material limits. It is not uncommon for the inflation shock loads to exceed two or three times the nominal load of the parachute. By moderating inflation rates, reefing reduces peak loads and promotes a more uniform distribution of stress throughout the canopy and suspension system. This is particularly important given the susceptibility of parachute structures to localized stress amplification at seams, joints, and stitched elements, making reefing a key design feature for ensuring structural integrity and reliable performance.

Despite the maturity of parachute design methodologies, many legacy approaches remain rooted in steady or empirically derived models that are not fully equipped to capture the highly transient and nonlinear nature of parachute deployment and inflation. Legacy design practices often rely on simplified load factors or empirical opening shock coefficients, which can obscure localized phenomena. In reality, the load path is highly non-uniform, leading to amplification at stress concentration points such as seams, reinforcements, and stitched interfaces. These localized stress intensifications are frequently the governing factors in material failure and structural integrity. Accurately predicting these effects requires resolving the coupled dynamics of fabric deformation, air inflation, and load redistribution – capabilities that extend beyond traditional design frameworks and motivate the need for high-fidelity, time-resolved FSI simulations, which have matured substantially in the last decade.

In this paper, we will focus on key aerodynamic interaction elements that are critical (or very important) but poorly understood or modeled using current state-of-the-art FSI simulation methods, and we will not discuss the very important structural mechanics modeling component that is crucial for successful computer-based prediction of parachute performance.

2 Computational Methodology

Figure 2 shows a diagram of a typical full-scale system FSI simulation framework with all the interacting elements. Flow, structure, suspension lines (usually described as cables), contact mechanics, and turbulence modeling are usually integrated into an adaptive-resolution (or mesh refinement) infrastructure to accommodate the large deformation of the parachute (Hornung & Kohn, 1998). In this figure, “dynamic topology” denotes the possibility of user actions during a simulation, such as reefing lines being cut or other actions that may be desired (e.g., releasing pilot parachutes).

The presence of large displacements and deformations makes conforming grids impractical, and most existing approaches use an immersed geometry coupling technique between the flow and the structure to circumvent regridding (Stein *et al.*, 2000; Peskin, 2002; Balaras, 2004; Mittal & Iaccarino, 2005; Kim & Choi, 2006; Kim & Peskin, 2009; Tezduyar *et al.*, 2010; Sawada, 2018; Mo *et al.*, 2018; Yu & Pantano, 2024). In this methodology, the fluid is typically solved on a fixed (Eulerian) background grid that does not conform to the instantaneous geometry of the parachute. The structural components (such as the fabric canopy and suspension lines) are represented independently in a Lagrangian finite element model (membrane or shell description) and allowed to move freely within the fluid mesh. Coupling between the two systems is then enforced through the exchange of forces and kinematic constraints across the fluid-structure interface. At each time step, the position and velocity of the structural surface are communicated to the fluid solver, which imposes appropriate boundary conditions – such as no-slip or slip conditions – through forcing terms, interpolation schemes, or modified flux calculations near the immersed boundary. In turn, the fluid solver computes pressure and viscous stresses in the vicinity of the structure, which are then projected back onto the structural mesh to determine the loads driving deformation. This bidirectional coupling enables the simulation of strongly nonlinear interactions without the need for continuous remeshing of the fluid domain. However, this convenience comes with important limitations. Because the fluid grid does not conform to the structural surface, the representation of the interface is inherently diffuse, often spanning several grid cells. As a result, sharp gradients in pressure and shear stress near the fabric surface are smeared, reducing the accuracy of load prediction, particularly in regions where boundary layer development, flow separation, or vortex shedding are critical. Additionally, accurately enforcing boundary conditions on highly flexible, thin structures remains challenging, especially when the local mesh resolution is insufficient relative to the scale of structural features such as seams or folds, or when wrinkling of the fabric is present. Despite ongoing advances, this loss of near-interface fidelity persists and is an accepted limitation of current immersed approaches, representing a key trade-off between computational tractability and physical accuracy in large-deformation FSI simulations. Nevertheless, the limitations of embedding geometry approaches are not particularly critical in fully deployed parachute simulations because, as we will discuss shortly, the majority of the load is due to pressure in a largely inviscid process.

To conclude, it should be noted that, in practice, self-contact mechanics is one of the most time-consuming computational components in parachute deployment simulations. Self-contact is very common when the parachute is still partially folded (coming out of its bag). By nature, contact resolution is highly geometric (it is, in principle, an NP problem), and specialized algorithms are required to address this

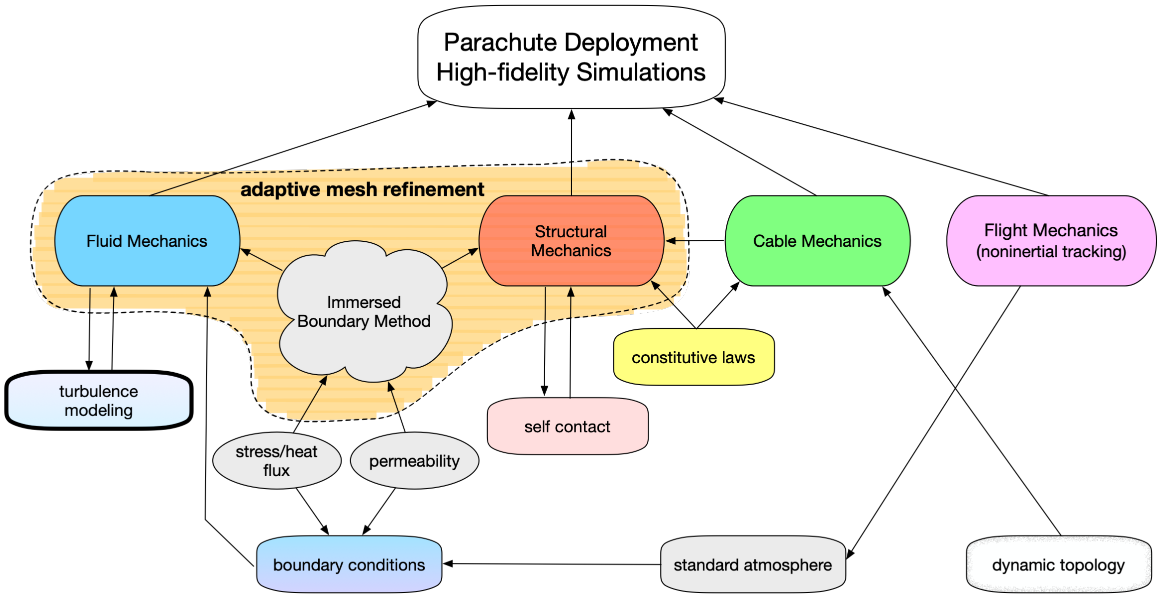

Figure 2. Diagram of the interactive elements involved in a fully-coupled parachute simulation.

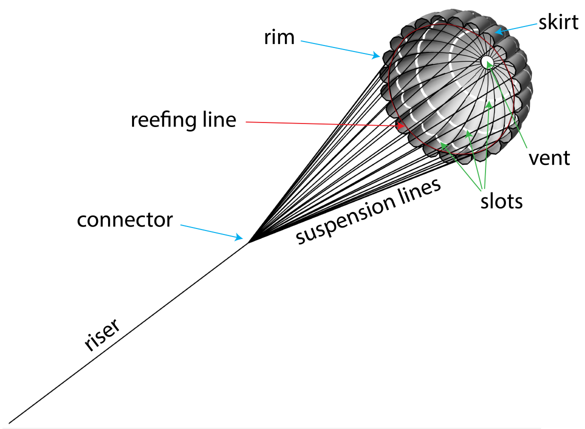

Figure 3. Schematic of a drogue parachute model used by the Orion CPAS.

mechanical feature in a reasonable amount of time. Physically correct deployment simulations are virtually impossible without such algorithms, e.g., see Wang & Pantano (2024).

3 Essential Elements of a Parachute

Here, I focus on subsonic canopies at high Reynolds numbers, but specialized supersonic parachutes are also used in military and space exploration applications (Lingard & Darley, 2005; Cruz & Lingard, 2006; Barnhardt *et al.*, 2007; Karagiozis *et al.*, 2011; Huang *et al.*, 2020). I also do not discuss low-speed (Stokes) parachutes or the fascinating applications of parachute clusters or parachute interactions with other bodies (e.g., dropping off from an aircraft). Figure 3 shows a realistic, simplified drogue parachute model used in the Orion vehicle Capsule Parachute Assembly System (CPAS) (Bledsoe *et al.*, 2009; Olmstead *et al.*, 2009). The real parachute in this application is a conical ribbon parachute (see Knacke (1991) for a comprehensive classification of parachutes), but it was simplified to a ringslot geometry to aid in simulations (reduce complexity). Most parachutes have features such as vents and slots, usually referred to as geometric porosity (in addition to the proper fabric porosity), that are intentionally incorporated to regulate internal pressure, reduce instabilities (e.g., pendulum-type oscillations), and prevent excessive shock load buildup during inflation. In the figure, one can see the suspension lines coming off the skirt of the parachute. Generally, the suspension lines run continuously around the canopy to ensure safety by eliminating the need for hard attachments to the canopy (preventing stress concentration regions where failures tend to occur). The suspension lines come together at a connector that attaches them to a riser line (specific to this type of parachute), going all the way to the payload. There are multiple mechanical attachments and connector types, each specialized for a given application. This geometry also features a reefing line that controls the opening of the parachute during deployment, preventing excessive shock load during initial inflation. Reefing lines are cut at pre-programmed times using a pyrotechnic cutter or similar device; a parachute can have multiple reefing lines of different lengths. The geometry shown in the figure is what is called the constructed geometry. This is not the actual shape of the parachute when it deploys, since it does not incorporate the elasticity of the fabric.

The aerodynamic parameters entering the problem are: the fluid density, ρ_∞, the system (freestream flow) velocity, U_∞, the dynamic viscosity, μ, and the parachute diameter D_o (e.g., the constructed geometry diameter). The canopy has a characteristic elastic modulus, E, thickness, h, and density ρ_s. Several other nondimensional parameters, such as the Poisson ratio, ν, and other characterizations of nonlinearity, are not considered qualitatively dominant here (but they do matter quantitatively). Furthermore, the suspension lines have a cable stiffness constant K_s (units of force), independent of their length L. Thermo-elastic effects that could couple with the fabric mechanics are not considered in this analysis, as they are relevant only in some high-speed (supersonic) parachutes. We also have gravity, g, and the payload mass, M_p, but one can simplify the dimensional analysis by assuming the parachute moves in an infinite-inertia medium and match the payload mass from the corresponding drag. The finite inertia effects associated with the deceleration of the system operate on a larger timescale, as inferred from the available parameters, than those of the aerodynamics. Using the standard conventions, we can define a Reynolds number

$$Re_o = \frac{\rho_\infty U_\infty D_o}{\mu}, \tag{1}$$

and a dynamic to elastic ratio, called a Cauchy number, of the canopy

$$Ca_c = \frac{\rho_\infty U_\infty^2}{E}. \tag{2}$$

In the applications of interest here, $Re_o \gg 1$ and $Ca_c \ll 1$, which result in a modest flow ability to stretch the fabric (small strains), although the cumulative (finite) stretch of the whole fabric can be substantial. But this does not imply small displacements of the canopy; on the contrary, aerodynamic forces move the canopy until the fabric is in tension. The relative motion is controlled by the ratio of inertia of the flow to the structure, which can be parameterized by a nondimensional mass, defined by

$$m^* = \frac{\rho_s h}{\rho_\infty D_o}, \tag{3}$$

which is very small in parachute applications. This implies that the flow can easily displace the canopy until a structural arrangement is reached in which the elastic forces dominate and therefore arrest further motion. In addition, we also have the true permeability of the fabric, which is usually parameterized as a velocity of flow through the fabric, v_s, as a function of the pressure drop across the fabric Δp; in general, it also depends on the amount and direction of stretch. For Darcy-type approximation, we have $v_s = k/\mu \Delta p$, where k is the intrinsic permeability (units of length squared). Computational studies suggest that permeability can reduce drag by up to 20%, depending on the fabric and parachute (it is not straightforward to test this effect in an experimental setting because one cannot usually choose the permeability of the fabric at will).

Finally, the large-scale oscillatory (bouncing) motion of the parachute is produced by the interaction between canopy pressurization and the elastic resistance of the suspension lines. This allows us to define a Cauchy number for the suspension lines, as the ratio of these forces, given by

$$Ca_s = \frac{\rho_\infty U_\infty^2 D_o^2}{K_s}, \tag{4}$$

which is typically of order unity. By comparing the inertia of the mass of fluid surrounded by the canopy with the cable stiffness of the suspension lines, it is possible to deduce a natural frequency of oscillation of the system, given by

$$\omega_p = \sqrt{\frac{K_s}{\rho_\infty D_o^3 L}}, \tag{5}$$

which is on the order of a second in many typical cases. These are the elementary parameters qualitatively defining the dynamics of parachutes. Other minor parameters entering the analytical analysis of parachutes are the Mach number, the ratio of bending to stretch energy of the fabric, Föppl-von Kármán number, defined as $h^2\kappa^2/\varepsilon^2$, where κ and ε denote the curvature and strain of the fabric, respectively. Bending is important primarily when wide wrinkling is present or when canopy tension disappears, e.g., during early deployment and inflation. Furthermore, the mass of the suspension lines, defined in terms of their line density ρ_c, anisotropy (warp vs weft stiffness) of the fabric, material damping coefficient (a quantity that is poorly understood for fabrics), and bending and torsion of the suspension lines. And finally, the properties of the payload, usually related to a Froude number, $Fr = U_\infty/\sqrt{gD_o}$, and atmospheric conditions, such as wind gust strength, parachute packing type, and, for high-altitude parachutes, variations in atmospheric density as the parachute falls, can also be important.

4 Key Aerodynamic Processes

The primary mechanism driving parachute inflation is the gradual pressurization of the canopy (Peterson *et al.*, 1996). Once the parachute is extracted from its deployment bag (typically by a pilot parachute or mortar), the canopy begins to unfurl, exposing increasing surface area to the oncoming flow. As air enters the canopy, it increases the internal (with respect to the external) pressure on portions of the fabric, causing the structure to expand outward. This process is highly transient and nonlinear: the canopy does not inflate uniformly, but rather through a sequence of localized filling, lobe formation, and spreading, influenced by fabric permeability, porosity, geometric constraints, and viscous processes (such as unsteady turbulent boundary layer interactions) (Peterson *et al.*, 1996). The balance between incoming mass flow, internal pressurization, and fabric tension governs the rate and stability of inflation. During the initial phase, the suspension lines are usually not in tension, and it is only after the canopy has traveled sufficiently behind the payload and partially inflated that one reaches the line-stretch condition, in which the suspension lines can transmit the load to the payload. The inflation process is strongly coupled to the structural response of the fabric once line-stretch is reached. As internal pressure rises, the canopy stretches and changes shape, further altering the flow field and the distribution of aerodynamic loads. This feedback loop between fluid loading and structural deformation is the essence of the fluid-structure interaction during inflation. Ultimately, full inflation is achieved when the canopy reaches equilibrium, in which aerodynamic forces, internal pressure, and structural tension are balanced. However, the path to this state involves complex unsteady flow phenomena, e.g., flow separation, vortex shedding, and transient jetting through vents. These processes significantly influence the dynamics of inflation, the load history, and the overall performance of the parachute system. It is no understatement to say that the substantial complexity of parachute design and modeling stems from their constantly evolving geometry.

By and large, the steady-state configuration of a parachute can be predicted by an inviscid calculation, since it is primarily controlled by the overpressure inside the parachute, which is not a viscous process (it results from the conversion of momentum into static pressure at the walls of the parachute). A few older studies and other anecdotal results suggest that up to 95% of the load on a fully inflated parachute can be predicted by an Euler (inviscid) simulation if the fabric (and other structural elements) response is correctly incorporated into the model. This does not apply to the deployment and inflation phases, since viscous aerodynamic effects, e.g., turbulent wake and boundary layer interactions, affect the inflation dynamics, or

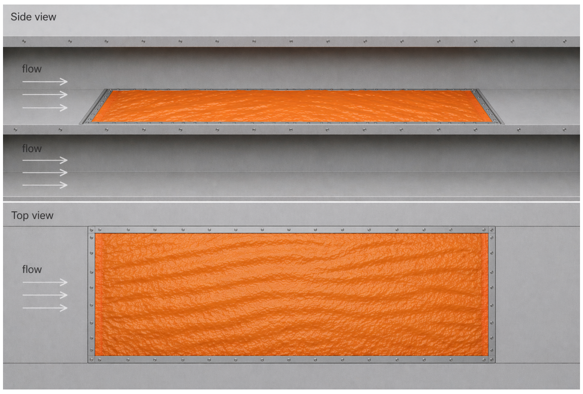

Figure 4. Sketch of turbulent boundary layer-fabric interaction setup.

when forebody wake interactions with the canopy are important. In principle, one can identify several elementary physical processes that often necessitate modeling: first, canopy-(turbulent) boundary layer interactions; second, interaction of the payload wake with the canopy; and finally, the inertial and aerodynamic forces of suspension lines. The relative importance of the three elementary processes depends on the stage in the life cycle of a parachute. During inflation, all processes are important, whereas the effects of suspension line inertia and aerodynamics are very minor in the fully inflated regime (except, possibly, in supersonic applications, where conical shockwaves have been observed emanating from the suspension lines, see Sengupta *et al.* (2008, 2009)). In terms of fundamental aerodynamic effects relevant to FSI, one can think of three processes that can be isolated from the complexity of a full parachute and, in principle, could be studied (more or less) separately.

4.1 Turbulent boundary layer/fabric interaction

The most elementary fluid-dynamic process is the interaction between turbulent boundary layers and the fabric. Figure 4 depicts such a configuration; NASA Ames has made some attempts at this problem. This arrangement is driven by boundary layers that exist independently of the fabric and are generated upstream of it. The energy driving the fabric motion is therefore provided by the unsteadiness of the flow. The physical parameters of this application are substantially different from those widely investigated in the past for stiff metallic panels subject to aerodynamic loads, e.g., in the study of flutter. Here, the fabric is very flexible, and there is flow above and below it. Furthermore, the pressure of the two streams can differ substantially, leading to some flow through the fabric due to its porosity. In a carefully designed experiment or simulation, one can also incorporate the tensile state of the fabric to differentiate flow phenomena at the skirt of the parachute from those at the back disk, where the tension may be larger because the transmural (difference in) pressure is greater.

The main quantity one would like to understand is the response of the wall shear stress, τ_w, as a function of fabric parameters and turbulence levels. Large-eddy simulation (LES) with wall closure is the only currently feasible high-resolution method in this application (Piomelli & Balaras, 2002; Bose & Park, 2018). Therefore, providing a reasonable good wall shear stress closure is the best way to improve modeling. Nevertheless, one should be aware that most canopy-flow interactions during deployment are not in equilibrium, and that strong pressure gradients and non-inertial effects play a large role in the dynamics of the fabric (and the flow) during canopy inflation. It should also be noted that there is a wide-scale distribution of fabric deformations, with the presence of large-scale waves (usually arranged along the main direction of flow) and low-scale wrinkling. This also depends on the relative direction and strength of the flow on each side of the fabric and the tensile state of the fabric.

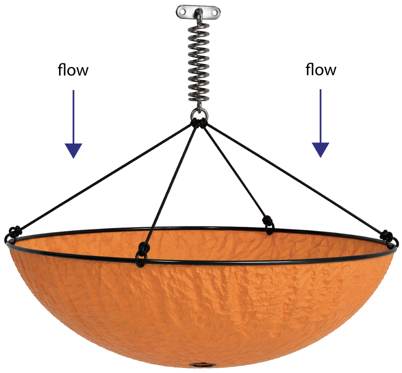

Figure 5. Sketch of a setup for the study of dynamic loading of a canopy.

4.2 Canopy aerodynamics coupling to suspension lines

The second elementary truly FSI problem is the dynamic loading of the canopy and its spring-like bouncing motion due to the elastic response of the suspension lines (and noninertial effects). A prototypical configuration is shown in figure 5. Here, the flow from top to bottom provides loading on a hemispherical cap, which generates its own wake and source of unsteadiness, resulting in unsteady loading and elastic energy being phased in and out of the spring. This is a surrogate problem for the study of shock-load dynamics and oscillations, which is difficult to achieve in a controlled experiment with a full-model parachute within the confines of a wind tunnel. The hemispherical cap can include a back vent and other openings to mimic the geometry of the parachute of interest. A metric of successful modeling is the ability to accurately predict the dynamic oscillation of the canopy, amplitude, and frequency, as a function of the physical parameters. The configuration should be tested both in standalone mode and also with a forebody object generating a wake that is ingested by the hemispherical cap. Many variations are possible depending on the ultimate application. This setup requires a stationary vertical wind tunnel. Note that the canopy will also experience lateral motion, in addition to axial (up-and-down) oscillation. It is also possible to generate too large oscillations due to the accumulation of elastic energy in the spring (extracted from the flow). Therefore, a damping mechanism may be needed at the spring, which should be connected to a loading cell to extract force and moments for analysis. Furthermore, it is known that the wakes behind flexible blunt geometries like this one are weaker than those behind rigid bodies; the Kármán street is not as pronounced (Kramer *et al.*, 2013). There are many interesting aerodynamic and FSI interactions worth investigating in this setup.

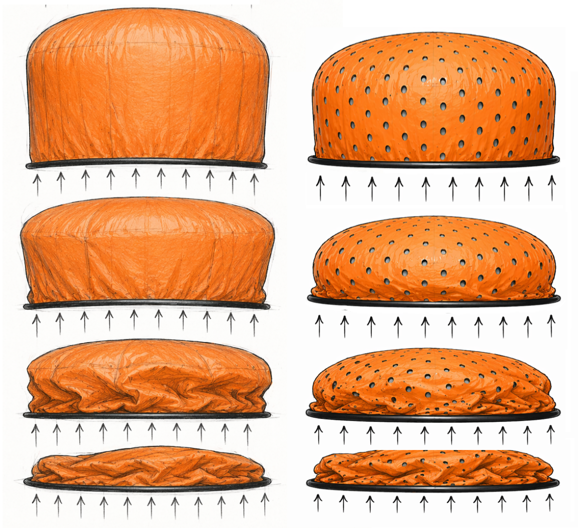

Figure 6. Sketch of bag inflation setup without (left) and with (right) openings.

4.3 Bag Inflation dynamics

Finally, the ultimate setup relevant to parachute inflation as a canonical FSI problem is the inflation of a bag. This is depicted in figure 6. The process is transient and triggered by the startup of a jet from the bottom of the figure (this arrangement avoids the lateral gravitational bias when inflating a parachute in a horizontal wind tunnel). The setup resembles the much-studied problem of airbag inflation, except that the inflation is now controlled by interaction with an unsteady jet (that is larger than the bag diameter), rather than by the release of gas in an enclosed airbag triggered by a pyrotechnic device. The aspect ratio of the bag, as well as the selection of fabric, should be chosen to approximate the parachute of interest. Flow velocity can be varied to investigate different deployment velocities, and a non-uniform jet can be used to elucidate inflation failures as a function of flow interactions with the bag. Keep in mind that some parachutes inflate in the wake of an aircraft, and the flow need not be simple ahead of a parachute during deployment.

The studies should be approached statistically because there are substantial deterministic reproducibility issues with this problem. There is little hope of manufacturing a perfectly defined crumbled bag; instead, random arrangements should be tested and compared with simulations to determine average inflation times, fabric tensioning, and loading of the attachment ring. This problem, due to its complexity, has received no attention as far as we are aware.

5 Example of Parachute Cluster Simulation

We used FSI to simulate the inflation phase and dis-reefing of the CPAS drogue parachute cluster (Taylor *et al.*, 2007) from a partially inflated state. These parachutes are used during the atmospheric entry of the Orion spacecraft as an intermediate decelerator before deploying the main parachutes, see Sengupta *et al.* (2012) for experimental results. The drogue parachute has a diameter $D_o = 4.48$ m in its constructed geometry, Young's modulus between 0.8310 GPa and 1.1805 GPa, thickness between 6.858×10^{-5} m and 1.8288×10^{-4} m for the four rings, respectively. We simulate the inflation process at the standard atmospheric condition at 4000 m (i.e., $\rho_\infty = 0.8194$ kg/m^3, $p_\infty = 61660$ Pa, $\mu = 1.661 \times 10^{-5}$ kg/(m s),

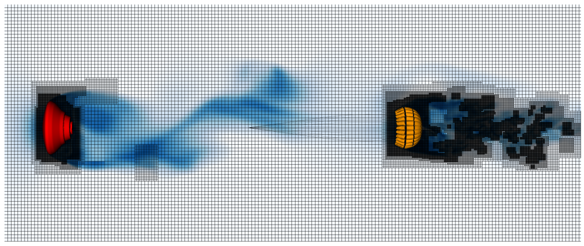

Figure 7. Grid refinement example for capsule-parachute simulation. Darker regions denote finer grids.

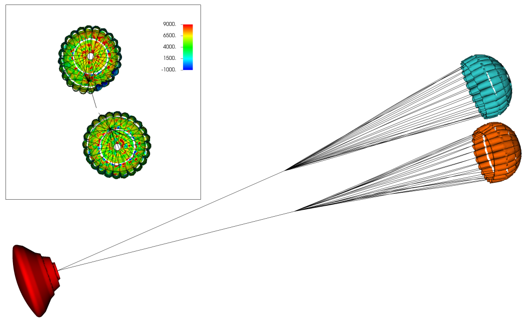

Figure 8. Parachute cluster at one instant in time just before dis-reefing. Flow runs from left to right in an inertial frame of reference (no deceleration). The inset depicts the transmural pressure on the canopies (in Pa) when viewed from the capsule attachment point.

Prandtl number is fixed to 0.7) and the Mach number is 0.3, which are within the flight envelope of the CPAS drogue parachute.

Each drogue parachute is discretized with 12,864 triangles with the subdivision thin-shell finite-element method, and structured adaptive mesh refinement (AMR) is used in the fluid, with the grid width at the coarsest level $\Delta x = 15.625$ cm and three additional refined grid levels with refinement ratio 2, making the smallest grid spacing equal to 1.95 cm. The AMR strategy is driven by local velocity gradients and proximity to the canopy. As illustrated in Fig. (7), the computational grid is significantly refined in regions surrounding the parachute and capsule, while remaining coarser elsewhere. This targeted refinement yields substantial computational savings relative to a uniformly fine grid and supports the efficiency of the methodology. The wake downstream of the capsule has not been further refined for simplicity in the present simulation. Complete descriptions of the computational formulation and algorithms can be found in Yu *et al.* (2019) and Yu & Pantano (2022, 2024).

In the actual application, the drogue parachutes are mortar-deployed, with a reefing line at the skirt of the parachute to control their inflation (Olmstead *et al.*, 2009; Morris *et al.*, 2011). The length of the reefing line increases at some point to a second-stage reefing before fully dis-reefed. In the simulations, it is not computationally practical to start the FSI simulations from the mortar deployment state; instead, we start from a configuration of the parachute that is semi-collapsed and resembles the parachute package after the mortar shooting and before full inflation (see Wang *et al.* (2022) case 1-band R1-C1). The parachute is initially frozen in this shape while the flow is initialized for approximately 1s. This initial flow simulation with the frozen parachutes is conducted until the flow is fully developed and the turbulence has approx-

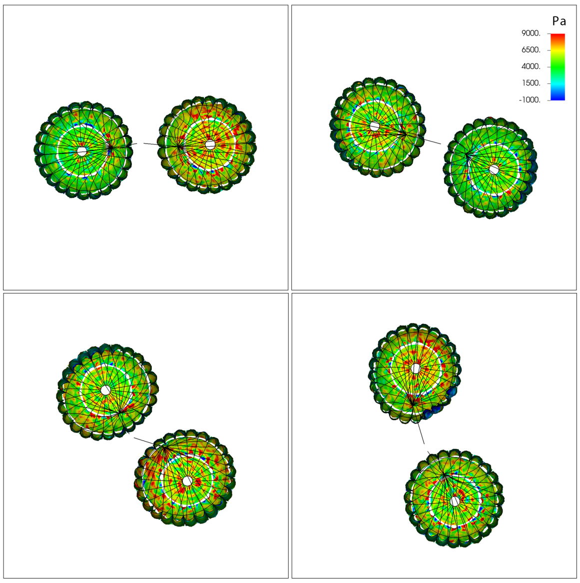

Figure 9. Cluster dynamics of parachutes in reefed configuration at times 1.25s, 1.5s, 1.75s and 2s, from top left to right to bottom left to right.

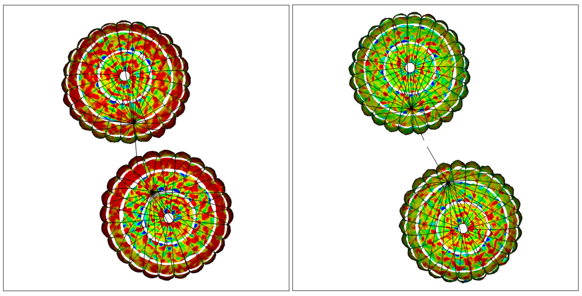

Figure 10. Canopy changes during dis-reefing, at peak load, (left) and relaxed after transient die out (right).

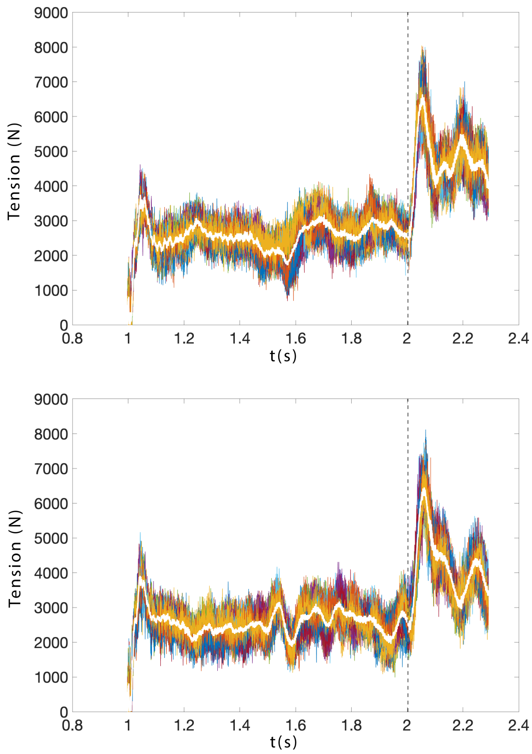

Figure 11. Parachute cluster suspension lines tension as a function of time. Thick white curves denote the average load of all the suspension lines (multicolor).

imately reached stationary conditions. The parachute is then allowed to deform, and a full FSI simulation is conducted. In the present simulation, the reefing line length is initially set to about 69% of the reference diameter of the parachute skirt, and fully cut 1s later. A more detailed study of the FSI of a single drogue parachute can be found in Yu *et al.* (2022). Fig. (9) shows the axial rotation dynamics of the parachute cluster while in reefed configuration. Contour plots of transmural pressure are overlaid on the canopy with the range shown in the colorbar. Note that the parachutes are stable and never interact too closely (no contact was detected between the canopies, in agreement with experimental observation), but their wakes do interact. Fig. (10) shows the canopies and transmural pressures, soon after dis-reefing, at the time of peak load, and soon thereafter when the canopy has re-stabilized, where the increase in canopy size is evident.

We finally report the transient dynamics of the suspension loads (which are directly related to the drag) between different reefing stages. Removing the reefing line allows the canopy to further inflate and change shape rapidly. Fig. (11) shows the transient tension of the two parachutes, before and after dis-reefing. As can be seen, a more or less stationary suspension line tension exists between 1s and 2s. This is followed by a substantial shock load. On average (white curves), the tension rises from about 2500 N to a peak of 6500 N before relaxing back to about 4000 N in the unreefed state. Individually, the situation during the shock load is even larger, as several suspension lines reach about 8000 N. This is an example of a shock load that is still present even when using reefing and that impacts the design of parachutes in general.

6 Conclusions

Despite the challenges, the outlook for high-fidelity parachute simulation is far from pessimistic. Significant progress over the past two decades has been driven in part by the underlying physics of the problem: in the fully deployed state, the dominant contribution to drag arises primarily from conversion of flow momentum into pressure, rather than from viscous shear. As a result, even simulation approaches with limited near-wall resolution can provide reasonably accurate predictions of global performance metrics such as drag and descent rate once the canopy has reached a quasi-steady configuration. However, this relative success does not extend to the deployment and inflation phases. During these highly transient stages, the flow is strongly unsteady, with complex fluid-structure coupling, evolving topology, contact mechanics, and sensitivity to fabric properties, permeability, and initial conditions. Accurately capturing these processes remains a major challenge, and continued advances in modeling, numerical methods, and experimental validation are required to achieve reliable predictive capability in this critical regime. We discussed three key fluid-structure interaction problems that could help improve the state of the art in modeling currently lacking in this application. An example of a simulation of a cluster of two parachutes, corresponding to the drogue parachutes of the Orion capsule deceleration system, was presented to highlight current capabilities.

Acknowledgement

During the preparation of this work, ChatGPT™ (OpenAI), under license from the University of Southern California, assisted with the preparation of sketches and editing portions of the manuscript. All scientific content, modeling, and conclusions are the sole responsibility of the author. The parachute cluster simulation was conducted by H. Yu while a graduate assistant at the University of Southern California.

REFERENCES

Balaras, Elias 2004 Modeling complex boundaries using an external force field on fixed Cartesian grids in large-eddy simulations. *Computers and Fluids* **33** (3), 375–404.

Barnhardt, Michael, Drayna, Travis, Nompelis, Ioannis, Candler, Graham & Garrard, William 2007 Detached Eddy Simulations of the MSL Parachute at Supersonic Conditions. In *19th AIAA Aerodynamic Decelerator Systems Technology Conference and Seminar*, pp. 263–273. Reston, Virigina: American Institute of Aeronautics and Astronautics.

Bledsoe, Kristin, Englert, Megan, Morris, Aaron & Olmstead, Randy 2009 Overview of the Crew Exploration Vehicle Parachute Assembly System (CPAS) Generation I Main and Cluster Development Test Results. In *20th AIAA Aerodynamic Decelerator Systems Technology Conference and Seminar*, pp. 1–13. Reston, Virigina: American Institute of Aeronautics and Astronautics.

Bose, Sanjeeb T. & Park, George Ilhwan 2018 Wall-Modeled Large-Eddy Simulation for Complex Turbulent Flows. *Annual Review of Fluid Mechanics* **50** (1), 535–561.

Cockrell, D.J. 1987 The aerodynamics of parachutes. *Tech. Rep.* AGARD-AG-295. North Atlantic Treaty Organization.

Cruz, Juan R. & Lingard, J. Stephen 2006 Aerodynamic decelerators for planetary exploration: Past, present, and future. *Collection of Technical Papers - AIAA Guidance, Navigation, and Control Conference 2006* **8** (August), 5342–5361.

Hornung, Richard D. & Kohn, Scott R. 1998 The use of object-oriented design patterns in the SAMRAI structured amr framework. In *SIAM Workshop on Object-Oriented Methods for Inter-Operable Scientific and Engineering Computing*, pp. 235–244. Yorktown Heights, New York: SIAM.

Huang, Daniel Z., Avery, Philip, Farhat, Charbel, Rabinovitch, Jason, Derkevorkian, Armen & Peterson, Lee D. 2020 Modeling, Simulation and Validation of Supersonic Parachute Inflation Dynamics during Mars Landing. In *AIAA Scitech 2020 Forum*, , vol. 1 Part F. Reston, Virginia: American Institute of Aeronautics and Astronautics.

Karagiozis, K., Kamakoti, R., Cirak, F. & Pantano, C. 2011 A computational study of supersonic disk-gap-band parachutes using Large-Eddy Simulation coupled to a structural membrane. *Journal of Fluids and Structures* **27** (2), 175–192.

Kim, Dokyun & Choi, Haecheon 2006 Immersed boundary method for flow around an arbitrarily moving body. *Journal of Computational Physics* **212** (2), 662–680.

Kim, Yongsam & Peskin, Charles S. 2009 3-D Parachute simulation by the immersed boundary method. *Computers and Fluids* **38** (6), 1080–1090.

Knacke, T.W. 1991 Parachute recovery systems design manual. Technical Report 9207158. UD Navy, China Lake, CA 93555.

Kramer, R.M.J., Cirak, F. & Pantano, C. 2013 Fluid-structure interaction simulations of a tension-cone inflatable aerodynamic decelerator. *AIAA Journal* **51** (7), 1640–1656.

Lingard, John & Darley, Matt 2005 Simulation of parachute fluid structure interaction in supersonic flow. In *18th AIAA Aerodynamic Decelerator Systems Technology Conference and Seminar*, p. 1607.

Mittal, R. & Iaccarino, G. 2005 Immersed boundary methods. *Annual Review of Fluid Mechanics* **37**, 239–261.

Mo, Huangrui, Lien, Fue Sang, Zhang, Fan & Cronin, Duane S. 2018 An immersed boundary method for solving compressible flow with arbitrarily irregular and moving geometry. *International Journal for Numerical Methods in Fluids* **88** (5), 239–263.

Morris, Aaron, Bledsoe, Kristin, Fraire, Jr., Usbaldo, Moore, James, Ray, Eric & Olson, Leah 2011 Summary of CPAS Gen II Testing Analysis Results. In *21st AIAA Aerodynamic Decelerator Systems Technology Conference and Seminar*, pp. 1–14. Reston, Virigina: American Institute of Aeronautics and Astronautics.

Olmstead, Randy, Morris, Aaron, Bledsoe, Kristin & Englert, Megan 2009 Overview of the Crew Exploration Vehicle Parachute Assembly System (CPAS) Generation I Drogue and Pilot Development Test Results. In *20th AIAA Aerodynamic Decelerator Systems Technology Conference and Seminar*, pp. 1–14. Reston, Virigina: American Institute of Aeronautics and Astronautics.

Peskin, Charles S. 2002 The immersed boundary method. *Acta Numerica* **11**, 479–517.

Peterson, C W, Strickland, J H & Higuchi, H 1996 The fluid dynamics of parachute inflation. *Annual Review of Fluid Mechanics* **28** (1), 361–387.

Piomelli, Ugo & Balaras, Elias 2002 Wall-Layer Models for Large-Eddy Simulations. *Annual Review of Fluid Mechanics* **34** (1), 349–374.

Sawada, T. 2018 *Frontiers in Computational Fluid-Structure Interaction*, chap. Interface-reproducing capturing (IRC) technique for fluid-structure interaction: methods and applications, pp. 435–480. Springer Nature Switzerland.

Sengupta, Anita, Machin, Ricardo, Bourland, Gary, Longmire, Ellen, Ryan, Mitch, Haugen, Erik, White, Edward, Ross, James, Laguna, Jose, Sinclair, Robert, Hennings, Elsa & Bissell, Daniel 2012 Performance of a conical ribbon drogue parachute in the wake of a subscale Orion command module. *IEEE Aerospace Conference Proceedings* .

Sengupta, A., Roeder, J., Kelsch, R., Wernet, M., Kandis, M. & Witkowski, A. 2008 Supersonic disk gap band parachute performance in the wake of a Viking-type entry vehicle from Mach 2 to 2.5. In *AIAA Atmospheric flight mechanics conference and exhibit*. Honolulu, Hawaii.

Sengupta, A., Steltzner, A., Witkowski, A., Candler, G. & Pantano, C. 2009 Findings from the supersonic qualification program of the Mars Science Laboratory prachute system. In *20^{th} AIAA Aerodynamic Decelerator Systems Technology Conference and Seminar*. Seattle, WA.

Stein, Keith, Benney, Richard, Kalro, Vinay, Tezduyar, Tayfun E., Leonard, John & Accorsi, Michael 2000 Parachute fluid-structure interactions: 3-D computation. *Computer Methods in Applied Mechanics and Engineering* **190** (3-4), 373–386.

Taylor, Anthony P (Tony), Machin, Ricardo (Koki), Royall, Paul & Sinclair, Robert 2007 Developing the Parachute System for NASA's Orion: An Overview at Inception. In *19th AIAA Aerodynamic Decelerator Systems Technology Conference and Seminar*, pp. 772–786. Reston, Virigina: American Institute of Aeronautics and Astronautics.

Tezduyar, Tayfun E., Takizawa, Kenji, Moorman, Creighton, Wright, Samuel & Christopher, Jason 2010 Space-time finite element computation of complex fluid-structure interactions. *International Journal for Numerical Methods in Fluids* **64** (10-12), 1201–1218.

Wang, Q. & Pantano, C. 2024 A parallel geometric contact algorithm for thin shell finite elements in explicit time integration. *Computers and Structures* **305** (107567).

Wang, Q., Yu, H. & Pantano, C. 2022 Structural simulations of conical ribbon parachute deployment with a new detailed fabric contact algorithm, reefing line interactions and suspension line dynamics. In *26th AIAA Aerodynamic Decelerator Systems Technology Conference and Seminar*. Toulouse, France: American Institute of Aeronautics and Astronautics.

Yu, H. & Pantano, C. 2022 An immersed boundary method with implicit body force for compressible viscous flow. *Journal of Computational Physics* **459**, 111125.

Yu, H. & Pantano, C. 2024 A regularized projection immersed boundary method for smooth boundary forces. *Journal of Computational Physics* **496**, 112571.

Yu, H., Pantano, C. & Cirak, F. 2019 Large-Eddy Simulation of Flow Over Deformable Parachutes using Immersed Boundary and Adaptive Mesh. In *AIAA Scitech 2019 Forum*. Reston, Virginia: American Institute of Aeronautics and Astronautics.

Yu, H., Wang, Q. & Pantano, C. 2022 Wang *et al.* (2022). In *26th AIAA Aerodynamic Decelerator Systems Technology Conference and Seminar*. Toulouse, France: American Institute of Aeronautics and Astronautics.